18-Qubit Entanglement with Six Photons' Three Degrees of Freedom

Xi-Lin Wang, Yi-Han Luo, He-Liang Huang, Ming-Cheng Chen, Zu-En Su, Chang Liu, Chao Chen,
Wei Li, Yu-Qiang Fang, Xiao Jiang, Jun Zhang, Li Li, Nai-Le Liu, Chao-Yang Lu, and Jian-Wei Pan

*Hefei National Laboratory for Physical Sciences at Microscale and Department of Modern Physics,
University of Science and Technology of China, Hefei, Anhui 230026, China;
CAS Centre for Excellence in Quantum Information
and Quantum Physics, University of Science and Technology of China, Hefei, Anhui 230026, China;
and CAS-Alibaba Quantum Computing Laboratory, Shanghai 201315, China*

Full control of multiple degrees of freedom of multiple particles represents a fundamental ability for quantum information processing. We experimentally demonstrate an 18-qubit Greenberger-Horne-Zeilinger entanglement by simultaneous exploiting three different degrees of freedom of six photons, including their paths, polarization, and orbital angular momentum. We develop high-stability interferometers for reversible quantum logic operations between the photons' different degrees of freedom with precision and efficiencies close to unity, enabling simultaneous readout of $2^{18} = 262\,144$ outcome combinations of the 18-qubit state. A state fidelity of 0.708 ± 0.016 is measured, confirming the genuine entanglement of all 18 qubits.

Quantum information is encoded by different states in certain degrees of freedom (d.o.f.) of a physical system. For example, the quantum information of a single photon can be encoded not only in its polarization [1,2], and also in its time [3], orbital angular momentum (OAM) [4], and spatial modes [5]. A central theme in quantum information science is to coherently control an increasing number of quantum particles as well as their internal and external d.o.f., meanwhile maintaining a high level of coherence. The ability to create and verify multiparticle entanglement with individual control and measurement of each qubit serves as an important benchmark for quantum technologies. To this end, genuine multipartite entanglement has been reported for up to 14 trapped ions [6], ten photons [7,8], and ten superconducting qubits [9]. Very recently, the deterministic generation of complex states of 20 trapped-ion qubits and the detection of genuine multiparticle entanglement in groups of up to five neighboring qubits have also been reported [10].

The simultaneous entanglement with multiple d.o.f.—known as hyperentanglement [11]—offered an efficient route to increasing the number of entangled qubits [12,13], and enables enhanced violations of local realism [14,15], quantum superdense coding [16], simplified quantum logic gates [17], and teleportation of multiple d.o.f. of a single photon [18]. Previous experiments have demonstrated hyperentangled states of two photons in the form of product states of Bell states [12] and genuinely entangled Greenberger-Horne-Zeilinger (GHZ) [19] states with up to five photons and 2 d.o.f. [13]. However, it remained a technological challenge for the multiphoton experiments to go beyond 2 d.o.f.

To this end, we develop methods that allow not only scalable creations of hyperentanglement of multiple photons with 3 d.o.f., but also reversible conversion and simultaneous measurement of multiple d.o.f. with near-unity precision and efficiency. With these new techniques, we are able to demonstrate and confirm 18-qubit maximal entanglement in the GHZ state—the largest such state so far—by manipulating the polarization, spatial modes, and OAM of six photons.

We start by producing polarization-entangled six-photon GHZ states [20,21]. Three pairs of entangled photons are generated by beamlike type-II spontaneous parametric down-conversion [see Fig. 1(a)] where the signal-idler photon pairs are emitted as two separate circular beams, favorable for being collected into single-mode fiber [7]. The geometry of the down-conversion crystal, where a half-wave plate is sandwiched between two 2-mm-thick β-barium borates ensures that the obtained photon pairs are polarization entangled [7] in the form of $|\psi^2\rangle = (|H\rangle|V\rangle - |V\rangle|H\rangle)/\sqrt{2}$, where H (V) denotes the horizontal (vertical) polarization. The fidelities of the three pairs of entangled photons are measured to be on average 0.98 ± 0.01.

Next, we combine photons 1 and 3 on a polarization beam splitter (PBS) [22] and combine one of its outputs with photon 5 on another PBS [see Fig. 1(a)]. The PBSs transmit H and reflect V. Fine adjustments of the delays between the different paths are made so that the photons arrive at the PBSs simultaneously. All six photons are coupled into single-mode fibers and filtered by 3-nm interference filters [7]. Upon detecting one and only one photon in each output, the six photons are projected into
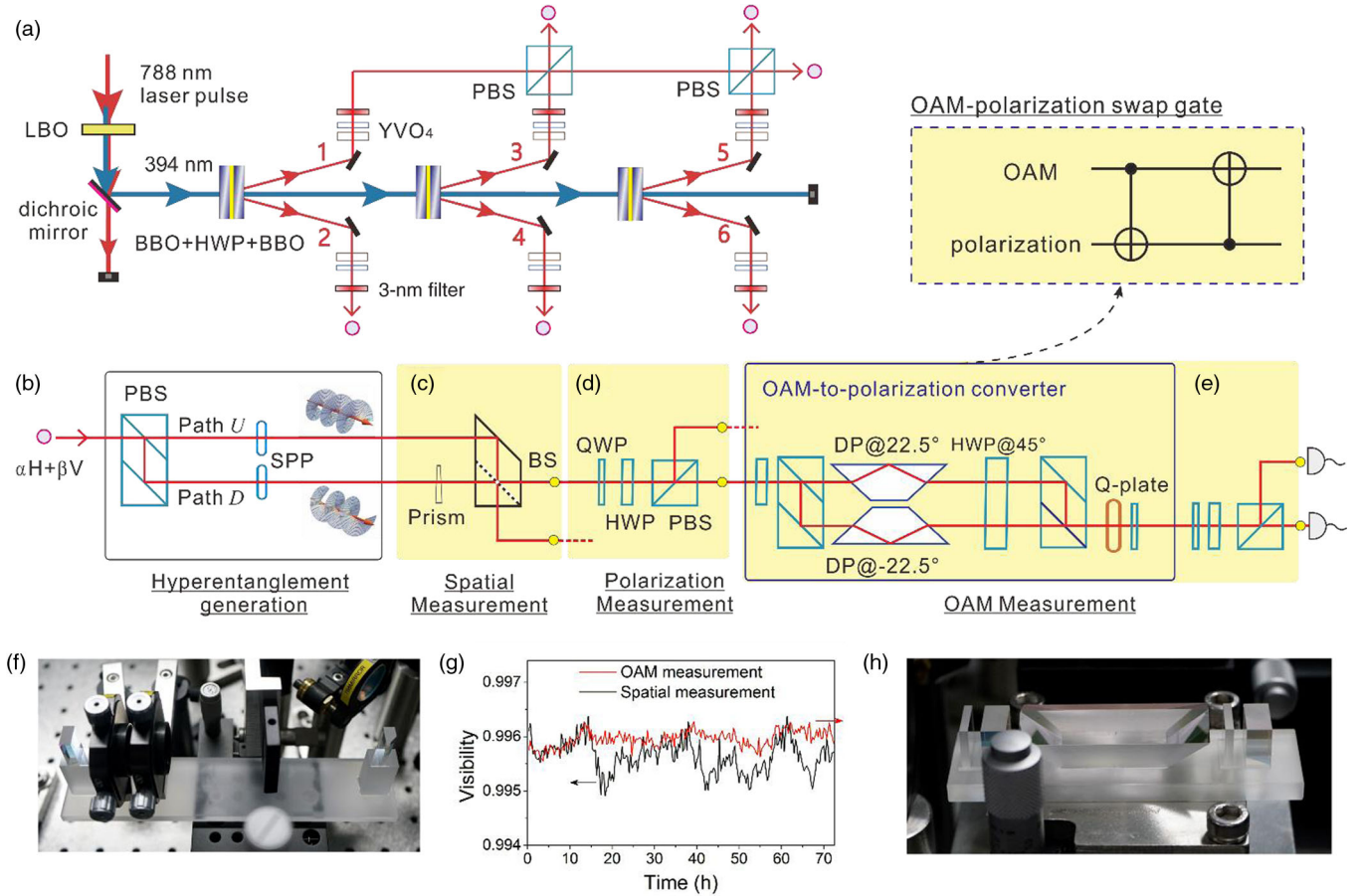
FIG. 1. Scheme and experimental setup for creating and verifying the 18-qubit GHZ state consisting of six photons and 3 d.o.f. (a) The generation of the six-photon polarization-entangled GHZ state. An ultrafast laser with a central wavelength of 788 nm, a pulse duration of 140 fs, and a repetition rate of 80 MHz is focused on a lithium triborate (LBO) and up-converted to 394 nm. The ultraviolet laser is focused on three custom-designed sandwichlike nonlinear crystals, each consists of two 2-mm-thick β-barium borates (BBOs) and one HWP to produce three pairs of entangled photons. In each output, two pieces of YVO_4 crystals with different thickness and orientation are used for spatial and temporal compensation for the birefringence effects. The three pairs of entangled photons are combined on two PBSs to generate a six-photon polarization-entangled GHZ state. (b) For each single photon, it is sent through a double PBS, and two SPPs to be prepared in a single-photon three-qubit state. (c) The measurement of the spatial qubit with closed (dash line) or open (without the dash line) interferometric configuration. (d) Polarization measurement. (e) High-efficiency and dual-channel OAM readout by coherently convert the OAM to polarization by a swap gate (inset). (f) Photo of the actual setup used in (b) and (c). By vertical translation, it is convenient to switch between open and closed (g). Real-time monitoring of the visibilities in the spatial (f) and OAM (h) measurements. (h) Photo of the actual setup used in (e). DP: Dove prism.

the GHZ state in the form of $|\psi^6\rangle = (|H\rangle^{\otimes 6} - |V\rangle^{\otimes 6})/\sqrt{2}$. We obtain a sixfold coincidence count rate of ~ 0.2 Hz in our experiment.

Thus far, only 1 d.o.f. of the photons is used. The information-carrying capacity of the photons can be vastly expanded by exploiting other d.o.f., including their spatial modes and OAM. To entangle the other d.o.f., we apply deterministic quantum logic gates on the single-photon's polarization and the other d.o.f. Experimentally, we first pass each single photon through a PBS which splits the photon into two paths denoted as up (U) and down (D) according to its polarization H and V, respectively. This process can be seen as a controlled-NOT (CNOT) gate where

the polarization acts as the control qubit and the path acts as the target qubit, which transforms an arbitrary unknown input single photon in the state $\alpha|H\rangle + \beta|V\rangle$ to a polarization-path hyperentangled state $\alpha|H\rangle|U\rangle + \beta|V\rangle|D\rangle$. Finally, we encode and entangle the OAM qubit to the photons. Inserting two spiral phase plates (SPPs) [23] in both paths transforms the photon in the U and D paths into right-handed and left-handed OAM of $+\hbar$ and $-\hbar$ which we denote as $|R\rangle$ and $|L\rangle$, respectively. Each photon is, thus, prepared in a hyperentangled state in the form of $\alpha|H\rangle|U\rangle|R\rangle + \beta|V\rangle|D\rangle|L\rangle$. By doing so, starting from the six-photon polarization-entangled GHZ state [Fig. 1(a)], we arrive at a hyperentangled 18-qubit GHZ state in the

form of $|\psi^{18}\rangle = (|0\rangle^{\otimes 18} - |1\rangle^{\otimes 18})/\sqrt{2}$, where for simplification, we denote $|H\rangle$, $|U\rangle$, and $|R\rangle$ as logic $|0\rangle$, and $|V\rangle$, $|D\rangle$, and $|L\rangle$ as logic $|1\rangle$.

The measurement of the 18 individual qubits that expand an effective Hilbert space to 262 144 dimensions and the verification of their multipartite genuine entanglement can be technologically more difficult than creating itself. All 18 qubits encoded in the 3 d.o.f. are to be measured both in the computational basis ($|0\rangle$, $|1\rangle$) and in the superposition basis $(|0\rangle \pm e^{i\theta}|1\rangle)/\sqrt{2}$ ($0 \leq \theta \leq \pi$). It is necessary to independently read out 1 d.o.f. without disturbing any other. The measurements are designed sequentially in three steps.

First, the spatial-mode qubit is measured using a closed or open Mach-Zehnder interferometer with or without the second 50:50 beam splitter [see Fig. 1(c)]. The open configuration is used to measure the ($|0\rangle$, $|1\rangle$) basis directly. The closed configuration together with a small-angle prism that adjusts the phase between the two paths is used to measure the $(|0\rangle \pm e^{i\theta}|1\rangle)/\sqrt{2}$ basis. The two outputs [labeled as yellow circles in Fig. 1(c)] of the open or closed beam splitter correspond to the two orthogonal projection results. In such measurements, the interferometers must be subwavelength stable. We design the beam splitters such that the output modes are parallel and displaced by only 6 mm [see Fig. 1(c)], and the beam splitters are glued on a glass plate [see Fig. 1(f)], making the setup insensitive to temperature fluctuations and mechanical vibrations. The current work used six such interferometers, which can remain stable for at least 72 h with observed visibilities exceeding 99.4%.

The second step is to perform the polarization measurement. As shown in Fig. 1(d), one of the outputs from the spatial measurement passes through a quarter-wave plate (QWP), a half-wave plate (HWP), and a PBS. By adjusting the QWP and HWP at angles of (0°, 0°) and (45°, 22.5° − $\theta/4$) with respect to the vertical axis, the measurement basis for the polarization states is set for the ($|0\rangle$, $|1\rangle$) basis and the $(|0\rangle \pm e^{i\theta}|1\rangle)/\sqrt{2}$ basis, respectively. After the PBS, the transmitted or reflected spatial modes correspond to two orthogonal projection outcomes.

The last step is the readout of the OAM, which, unlike the polarization, was known to be difficult to measure with high efficiency and two-channel output simultaneously [4,12,16,24–28]. Our method here is to deterministically map the OAM qubit to the polarization through two consecutive CNOT gates between the 2 d.o.f. that together form a quantum swap gate [see the inset of Fig. 1(e)]. In the first CNOT gate, the OAM acts as the control qubit and the polarization acts as the target qubit, which converts the initial state $(\alpha|R\rangle + \beta|L\rangle)|H\rangle$ to an entangled state $\alpha|R\rangle|H\rangle + \beta|L\rangle|V\rangle$. In our experiment, this is achieved by using an interferometer which consists of two double PBSs and two Dove prisms as shown in

Fig. 1(e) (see the Supplemental Material [29]). In the second CNOT gate, the polarization acts as the control qubit, and the OAM is the target qubit transforming the state $\alpha|R\rangle|H\rangle + \beta|L\rangle|V\rangle$ to $(\alpha|H\rangle + \beta|V\rangle)|R\rangle$. Thus, the difficult-to-measure OAM information is coherently transferred to the polarization, which can be conveniently and efficiently read out. Thus, for each single photon carrying 3 d.o.f., the measurement setup can give eight possible outcomes.

Finally, the OAM mode $|R\rangle$ is converted back to the fundamental Gaussian mode (denoted as $|G\rangle$) for efficient coupling into single-mode fibers. This task, together with the second CNOT gate, is completed using one element called the q plate [30]. It is an inhomogeneous anisotropic media that couples the polarization with the OAM, transforming $|R\rangle(|H\rangle - i|V\rangle)/\sqrt{2}$ to $|G\rangle(|H\rangle + i|V\rangle)/\sqrt{2}$, and $|L\rangle(|H\rangle + i|V\rangle)/\sqrt{2}$ to $|G\rangle(|H\rangle - i|V\rangle)/\sqrt{2}$, respectively (see the Supplemental Material [29]). We develop an integrated design for the OAM-to-polarization converter [see Fig. 1(h)] such that the 24 interferometers used in our work achieve an average visibility of 99.6%, keeping stable for over 72 h [see Fig. 1(g)]. Using this method, the overall efficiency of the OAM-to-polarization converter is 92%.

The complete experimental setup for creating and measuring the 18-qubit GHZ state is shown in Fig. S1 of the Supplemental Material [29], which includes 30 single-photon interferometers in total. The outputs are detected by 48 single-photon detectors and a complete set of 262 144 combinations can be simultaneously recorded by a coincidence counting system.

To demonstrate the genuie entanglement among the 3 d.o.f. of the N-qubit GHZ state, we first simultaneously measure all the qubits along the basis of $(|0\rangle \pm e^{i\theta}|1\rangle)/\sqrt{2}$ ($0 \leq \theta \leq \pi$). These measurements give rise to the experimentally estimated expectation values of the observable $M_\theta^{\otimes N} = (\cos\theta\sigma_x + \sin\theta\sigma_y)^{\otimes N}$. For the GHZ states, the expectation value of $M_\theta^{\otimes N}$ in theory fulfills $\langle M_\theta^{\otimes N}\rangle = \cos(N\theta)$, indicating an $N\theta$ oscillation behavior for the expectation value resulting from the collective response to the phase change of all the N entangled qubits. We test such behavior with the single-photon polarization state [Fig. 2(a)] and compare it to 3-d.o.f.-encoded GHZ states with one photon [Fig. 2(b)], four photons [Fig. 2(c)], and six photons [Fig. 2(d)], where the phase θ ramps continuously from 0 to π. The data are fitted to sinusoidal fringes that show an N-times increase in the oscillatory frequencies for the N-qubit GHZ states highlighting the potential of the hyperentangled states for super-resolving phase measurements [31].

The coherence of the 18-qubit GHZ state, which is defined by the off-diagonal element of its density matrix and reflects the coherent superposition between the $|0\rangle^{\otimes 18}$ and $|1\rangle^{\otimes 18}$ component of the GHZ state, can be calculated by
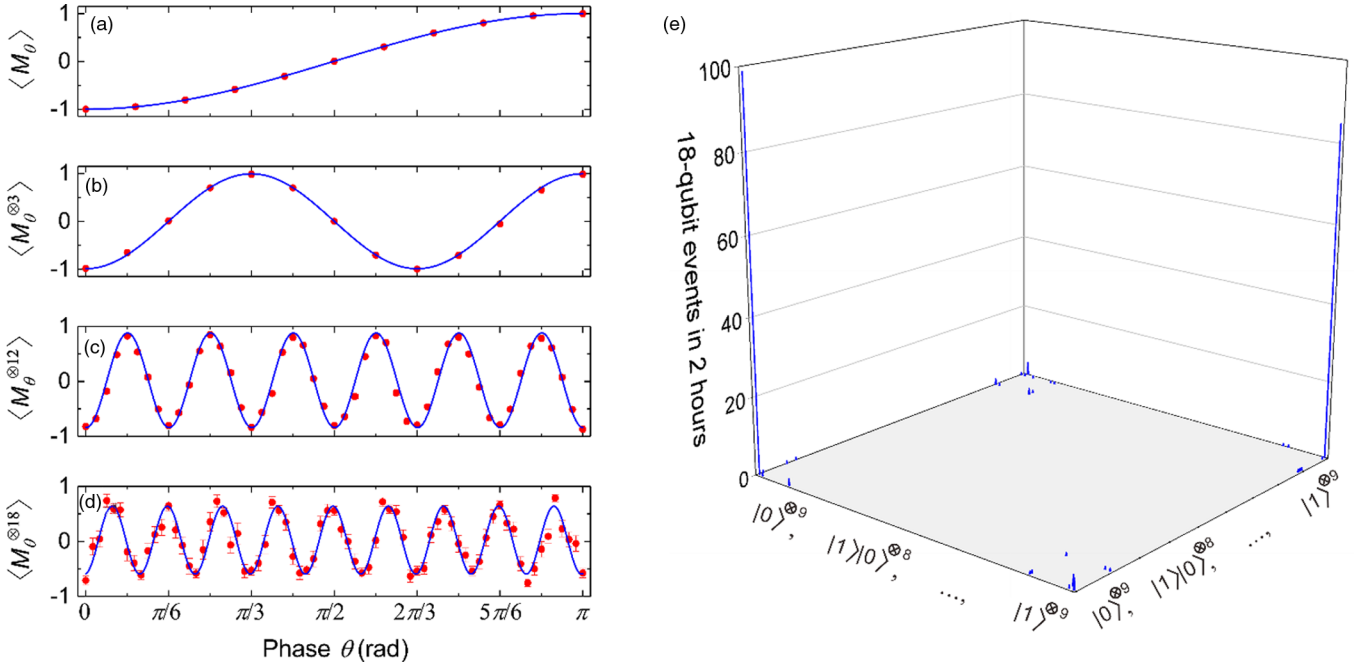
FIG. 2. Experimental data of 18-qubit GHZ entanglement. The (a) $N = 1$, (b) $N = 3$, (c) $N = 12$, and (d) $N = 18$ qubits are measured in the superposition base $(|0\rangle \pm e^{i\theta}|1\rangle)/\sqrt{2}$. Each of the N-qubit events corresponds to the observation of an eigenstate of the observable $M_\theta^{\otimes N} = (\cos\theta\sigma_x + \sin\theta\sigma_y)^{\otimes N}$ with an eigenvalue of $v_s = +1$ or $v_s = -1$. The expectation values $\langle M_\theta^{\otimes N}\rangle$ can be calculated by $\langle M_\theta^{\otimes N}\rangle = \sum_{s=1}^{2^N} p_s v_s$, where $p_s (s = 1, ..., 2^N)$ is the relative probability of the N-qubit detection events. The x axis denotes the phase shift θ between $|0\rangle$ and $|1\rangle$, and the y axis is the experimentally obtained $\langle M_\theta^{\otimes N}\rangle$. Error bars indicate 1 standard deviation and are calculated by the experimentally detected N-qubit events with the propagated Poissonian counting statistics. In (a)–(c), the error bars are smaller than the data points. (e) 18-qubit events in the computational $|0\rangle/|1\rangle$ basis accumulated for 2 h are displayed in a $512 \times 512 = 262\,144$ dimensional matrix.

$$\langle C^{18}\rangle = \frac{1}{18}\sum_{k=0}^{17}(-1)^{k+1}\langle M_{(k\pi/18)}^{\otimes 18}\rangle.$$

From the data shown in Fig. 2(d), the coherence is calculated to be 0.602 ± 0.019.

For a more detailed characterization of the experimentally created 18-qubit state, we further make measurements at the $|0\rangle/|1\rangle$ basis. For an ideal GHZ state, the correct terms in this basis should be $|0\rangle^{\otimes 18}$ and $|1\rangle^{\otimes 18}$ only. Our collected data for the 2^{18} combinations are plotted in Fig. 2(e). By comparing the registered coincidence counts, it shows that the $|0\rangle^{\otimes 18}$ and $|1\rangle^{\otimes 18}$ terms dominate the overall events, with a signal-to-noise ratio (defined as the ratio of the average of the two desired components to that of the remaining nondesired ones) of $5.7 \times 10^5 : 1$. Thus, we can calculate the population of the $|0\rangle^{\otimes 18}$ and $|1\rangle^{\otimes 18}$ terms as 0.814 ± 0.026. By analyzing the undesired components in Fig. 2(e), we estimate that $\sim 11.3\%$ noise is contributed from the double pair emission of parametric down-conversion noise and the remaining $\sim 7.3\%$ is from bit-flip error due to the imperfection of the optical elements such as the PBS and interferometers.

The state fidelity, which is defined as the overlap of the experimentally generated state with the ideal one is

$F(\psi^{18}) = \langle\psi^{18}|\rho_{\exp}|\psi^{18}\rangle = \text{Tr}(\rho_{\text{ideal}}\rho_{\exp})$. The fidelity can be directly calculated by the average of the expectation values of the population and coherence. From the experimental results as shown in Fig. 2, the fidelity of the generated entangled 18-qubit GHZ state is calculated to be 0.708 ± 0.016. The notion of a genuine multipartite entanglement characterizes whether generation of the state requires the interaction of all parties, distinguishing the experimentally produced state from any incompletely entangled state. For the GHZ states, it is sufficient for the presence of genuine multipartite entanglement [32] if their fidelities exceed the threshold of 0.5. Thus, with high statistical significance ($>13\sigma$), our experiment confirms the genuine 18-qubit entanglement, the largest entangled state demonstrated so far with individual control of each qubit.

In summary, we have developed methods for precise and efficient quantum logic operations on multiple d.o.f. of multiple photons and generated and verified the genuine entanglement among 18 qubits. Our work has demonstrated that combining multiparticle entanglement with multiple internal and external d.o.f. can provide an efficient route to increase the number of effective qubits. Using the same parametric down-conversion source, if only 1 d.o.f. (polarization) is exploited, an 18-photon GHZ state would have a count rate of 2.6×10^{-15} Hz. Exploiting 3 d.o.f., our

hyperentangled 18-qubit GHZ state is ~13 orders of magnitude more efficient than the single-d.o.f. 18-photon GHZ state. Our work has created a new platform for optical quantum information processing with multiple d.o.f. The ability to coherently control 18 qubits enables experimental access to previously unexplored regimes, for example, the realization of the surface code [33] and the Raussendorf-Harrington-Goyal code [34]. It will be interesting in future work to exploit the high quantum numbers [35–38] of the OAM or path to create a new type of entanglement [39].

[1] S. J. Freedman and J. F. Clauser, Phys. Rev. Lett. 28, 938 (1972).

[2] D. Bouwmeester, J. W. Pan, K. Mattle, M. Eibl, H. Weinfurter, and A. Zeilinger Nature (London) 390, 575 (1997).

[3] J. D. Franson, Phys. Rev. Lett. 62, 2205 (1989).

[4] A. Mair, A. Vaziri, G. Weihs, and A. Zeilinger, Nature (London) 412, 313 (2001).

[5] M. A. Horne, A. Shimony, and A. Zeilinger, Phys. Rev. Lett. 62, 2209 (1989).

[6] T. Monz, P. Schindler, J. T. Barreiro, M. Chwalla, D. Nigg, W. A. Coish, M. Harlander, W. Hänsel, M. Hennrich, and R. Blatt, Phys. Rev. Lett. 106, 130506 (2011).

[7] X. L. Wang, L. K. Chen, W. Li, H. L. Huang, C. Liu, C. Chen, Y. H. Luo, Z. E. Su, D. Wu, Z. D. Li, H. Lu, Y. Hu, X. Jiang, C. Z. Peng, L. Li, N. L. Liu, Y. A. Chen, C. Y. Lu, and J. W. Pan, Phys. Rev. Lett. 117, 210502 (2016).

[8] L.-K. Chen et al. Optica 4, 77 (2017).

[9] C. Song, K. Xu, W. Liu, C. P. Yang, S. B. Zheng, H. Deng, Q. Xie, K. Huang, Q. Guo, L. Zhang, P. Zhang, D. Xu, D. Zheng, X. Zhu, H. Wang, Y. A. Chen, C. Y. Lu, S. Han, and J. W. Pan, Phys. Rev. Lett. 119, 180511 (2017).

[10] N. Friis, O. Marty, C. Maier, C. Hempel, M. Holzäpfel, P. Jurcevic, M. B. Plenio, M. Huber, C. Roos, R. Blatt, and B. Lanyon, Phys. Rev. X 8, 021012 (2018).

[11] P. G. Kwiat, J. Mod. Opt. 44, 2173 (1997).

[12] J. T. Barreiro, N. K. Langford, N. A. Peters, and P. G. Kwiat, Phys. Rev. Lett. 95, 260501 (2005).

[13] W.-B. Gao, C. Y. Lu, X. C. Yao, P. Xu, O. Gühne, A. Goebel, Y. A. Chen, C. Z. Peng, Z. B. Chen, and J. W. Pan Nat. Phys. 6, 331 (2010).

[14] C. Cinelli, M. Barbieri, R. Perris, P. Mataloni, and F. De Martini, Phys. Rev. Lett. 95, 240405 (2005).

[15] T. Yang, Q. Zhang, J. Zhang, J. Yin, Z. Zhao, M. Żukowski, Z. B. Chen, and J. W. Pan, Phys. Rev. Lett. 95, 240406 (2005).

[16] J. T. Barreiro, T.-C. Wei, and P. G. Kwiat, Nat. Phys. 4, 282 (2008).

[17] B. P. Lanyon, M. Barbieri, M. P. Almeida, T. Jennewein, T. C. Ralph, K. J. Resch, G. J. Pryde, J. L. O'Brien, A. Gilchrist, and A. G. White Nat. Phys. 5, 134 (2009).

[18] X. L. Wang, X. D. Cai, Z. E. Su, M. C. Chen, D. Wu, L. Li, N. L. Liu, C. Y. Lu, and J. W. Pan Nature (London) 518, 516 (2015).

[19] D. M. Greenberger, M. Horne, A. Shimony, and A. Zeilinger, Am. J. Phys. 58, 1131 (1990).

[20] C. Y. Lu, X. Q. Zhou, O. Gühne, W. B. Gao, J. Zhang, Z. S. Yuan, A. Goebel, T. Yang, and J. W. Pan Nat. Phys. 3, 91 (2007).

[21] J. W. Pan, Z. B. Chen, C. Y. Lu, H. Weinfurter, A. Zeilinger, and M. Żukowski Rev. Mod. Phys. 84, 777 (2012).

[22] J. W. Pan, M. Daniell, S. Gasparoni, G. Weihs, and A. Zeilinger, Phys. Rev. Lett. 86, 4435 (2001).

[23] A. M. Yao and M. J. Padgett, Adv. Opt. Photonics 3, 161 (2011).

[24] E. Nagali, F. Sciarrino, F. DeMartini, L. Marrucci, B. Piccirillo, E. Karimi, and E. Santamato, Phys. Rev. Lett. 103, 013601 (2009).

[25] M. Hendrych, R. Gallego, M. Mičuda, N. Brunner, A. Acín, and J. P. Torres, Nat. Phys. 8, 588 (2012).

[26] B. C. Hiesmayr, M. J. A. de Dood, and W. Löffler, Phys. Rev. Lett. 116, 073601 (2016).

[27] Y. Zhang, M. Agnew, T. Roger, F. S. Roux, T. Konrad, D. Faccio, J. Leach, and A. Forbes Nat. Commun. 8, 632 (2017).

[28] M. Agnew, J. Z. Salvail, J. Leach, and R. W. Boyd, Phys. Rev. Lett. 111, 030402 (2013).

[29] Supplemental Material at http://link.aps.org/supplemental/10.1103/PhysRevLett.120.260502 for more information about the OAM-polarization CNOT gate, the q-plate and the experimental setup for creating and verifying a hyperentangled 18-qubit GHZ state.

[30] L. Marrucci, C. Manzo, and D. Paparo, Phys. Rev. Lett. 96, 163905 (2006).

[31] V. Giovannetti, S. Lloyd, and L. Maccone, Nat. Photonics 5, 222 (2011).

[32] O. Gühne and G. Toth, Phys. Rep. 474, 1 (2009).

[33] A. G. Fowler, M. Mariantoni, J. M. Martinis, and A. N. Cleland, Phys. Rev. A 86, 032324 (2012).

[34] R. Raussendorf, J. Harrington, and K. Goyal, New J. Phys. 9, 199 (2007).

[35] J. Leach, B. Jack, J. Romero, A. K. Jha, A. M. Yao, S. Franke-Arnold, D. G. Ireland, R. W. Boyd, S. M. Barnett, and M. J. Padgett Science 329, 662 (2010).

[36] R. Fickler, R. Lapkiewicz, W. N. Plick, M. Krenn, C. Schaeff, S. Ramelow, and A. Zeilinger Science 338, 640 (2012).

[37] M. Malik, M. Erhard, M. Huber, M. Krenn, R. Fickler, and A. Zeilinger Nat. Photonics 10, 248 (2016).

[38] Y. Zhou, M. Mirhosseini, D. Fu, J. Zhao, S. M. H. Rafsanjani, A. E. Willner, and R. W. Boyd, Phys. Rev. Lett. 119, 263602 (2017); X. Gu, M. Krenn, M. Erhard, and A. Zeilinger, Phys. Rev. Lett. 120, 103601 (2018).

[39] M. Krenn, M. Malik, R. Fickler, R. Lapkiewicz, and A. Zeilinger, Phys. Rev. Lett. 116, 090405 (2016).